A computational strategy for Eurocode 8 – compliant analyses of reinforced concrete structures by seismic envelopes

S. Sessa[a,*], F. Marmo[a], N. Vaiana[a], L. Rosati[a]

[a]*Department of Structures for Engineering and Architecture, University of Naples Federico II, Via Claudio, 21, 80124, Napoli, Italy*

Abstract

A procedure is presented for performing Eurocode 8–compliant spectral analyses of reinforced concrete structures by means of seismic response envelopes. To account for global torsion effects in the computation of the supreme envelope an algorithmic rotational response spectrum is defined. The presented strategy turns out to be particularly appropriate for finite element models including accidental eccentricity due to mass shifting since seismic envelopes can be computed by making reference to a single structural model rather than to separate models characterized by different signs of the accidental eccentricity. The proposed procedure is theoretically formulated and numerically tested by analyzing a rotationally stiff and a rotationally flexible building as well as two irregular structures. Moreover, it is compared with an alternative formulation derived from a recently proposed strategy concerning accidental torsion. The results show that the proposed procedure is coherent with the analysis procedures provided by standard codes and computationally more efficient.

Keywords: Response Spectrum method, Seismic envelopes, Three–Dimensional structure, Complete quadratic combination, response spectrum analysis

1. Introduction

Response spectrum analysis represents one of the most popular techniques in earthquake engineering practice [6] and is invariably considered by several build-

*Corresponding author
Email address: salvatore.sessa2@unina.it (S. Sessa)

ing codes [7], including [14], as the preferential strategy for the design of civil engineering structures. In this respect, multicomponent seismic responses play an important role in capacity check procedures in which the structural safety depends on the combination of more than a single response. This is the case of capacity checks of reinforced concrete beam sections with respect to axial force – biaxial bending [5, 24] and biaxial shear [35]. Moreover, in the case of three–component earthquake actions, it is essential to properly account for the randomness of the seismic input direction along which the design dynamic excitation is characterized [16, 21].

The previous aspects have been brilliantly addressed by the definition of Seismic Envelopes by [28, 29], based on the CQC3 modal superposition rule [27], which are capable to characterize multicomponent structural responses of spectral analyses accounting for the randomness of the earthquake directions and have been recently implemented in an optimization algorithm addressing for Eurocode 8–compliant capacity checks of Reinforced Concrete (RC) frame structures [36].

Despite of the efficiency of the procedure introduced by [28], the application of the Seismic Envelopes is limited to translational seismic actions since rotational components of the ground motion, and particularly global torsion, have not been explicitly included in the definition of seismic envelopes. Given the importance of global torsion in seismic analysis [19], this aspect compromises the application of the Seismic Envelopes in structural design because it is in contrast with code provisions and common practice.

In fact, several standard codes suggest to model the rotational seismic actions by defining an accidental eccentricity to be applied by shifting either floor masses or seismic static forces of the structure.

This is the case of New Zealand [34] seismic provisions, Canada [30] code and [14] whose prescriptions recommend mass shifting as the preferred strategy to account for global torsion. Moreover, building codes in countries such as Italian [32, 33] legally act as mandatory prescriptions so that the accidental eccentricity, intended as mass shifting, must be applied regardless of its theoretical and experimental background. For this reason, accidental eccentricity still represents the most widespread standard in common practice.

Such a strategy consists in increasing the natural eccentricity between the centers of mass and stiffness in order to take into account the random distribution of real masses as well as rotational components of the ground motion (see, e.g., [31, 10, 11, 8]). Eccentricity increment is usually defined as a function of the natural eccentricity and/or structural geometry. When performing a response spectrum analysis it is required, depending on specific code prescriptions, either to shift the

horizontal equivalent static forces or to move the floor masses of the prescribed accidental eccentricity.

Hence, the procedure is conceptually very simple, basically because it has been conceived for hand calculations, what was common in structural design till a couples of decades ago. On the contrary, its application turns out to be difficult if seismic responses are computed by means of seismic envelopes. In particular, the main limitation of using accidental eccentricity in combination with the Supreme Envelope consists in the necessity of addressing more than a single structural model. The envelope computation would be impossible otherwise since eccentric mass locations depend on the seismic input direction which cannot be defined *a priori* and depends on the response of interest.

A large variety of alternative strategies have been proposed to overcome the presence of more than a single structural model; in general, they consist in properly increasing the internal forces of a quantity depending on the elements' location and rotational behavior. Among the available strategies, the solution proposed by [15] and extended by [4] deals with flexible diaphragms while Eurocode 8 implements the strategy presented by [8].

Despite their computational efficiency, such procedures are limited to specific classes of buildings and are not capable to deal with shell elements. More in general, common design practice lacks of a unique strategy that can be applied to any kind of structural typology.

A very promising alternative approach, proposed by [3], consists in determining a rotational ground motion depending on the translational one and an accidental eccentricity defined by means of a static formulation alternative to the traditional one. Nevertheless, the strategy is based on theoretical assumptions whose coherence with code prescriptions should be verified after that a proper extension to response spectrum analysis is derived.

Differently from [3], this paper aims to present an alternative strategy for taking advantage of a suitably defined spectral characterization of rotational effects that provides equivalent or conservative results with respect to the code definition of accidental eccentricity. Being oriented to common practice structural design, it aims to be of easy application and to avoid any specialistic knowledge of rotational spectra. To this end, accurate modelling of rotational behavior can be sacrificed in favor of a simpler and computationally efficient strategy as long as approximations remain in a reasonably affordable range and/or results are conservative.

Aiming at a reliable and efficient modal–response spectrum analysis of structural models, at the same time compliant with code prescriptions, the proposed

approach allows the designer to deal with a single structural model since masses need not to be shifted from their original location, as in the classical accidental eccentricity approach.

Specifically, the proposed strategy is based on an envelope–spectral–analysis in which response spectra of horizontal ground motion components are combined with an algorithmic spectrum referred to the rotational motion about the vertical axis that suitably replaces the accidental eccentricity. Such a fictitious response spectrum does not characterize any physical ground motion since it is based on the equivalence between two mechanical oscillators defined for each modal shape.

In particular, the first *coupled* oscillator is characterized by an accidental eccentricity and is subject to a translational response spectrum defined by code prescriptions. The second *uncoupled* oscillator, having zero eccentricity, is subject to the translational excitation and to a fictitious rotational spectrum. The *algorithmic* rotational spectrum is computed so that equivalence in terms of rotational displacements of the two oscillators is fulfilled.

It is worth being emphasized that the proposed strategy is alternative as well to the procedure in which torsional moments, derived by equivalent static forces, are added at each floor. Remarkably, in contrast with the torsional moment procedure, the proposed strategy does not necessarily require the definition of rigid or semi-rigid floor diaphragms.

In order to investigate the effectiveness of the proposed approach, the algorithmic rotational spectrum introduced in the paper is compared with the strategy presented by [3] since this is the only one, among those previously quoted, to explicitly address the accidental eccentricity and capable of computing seismic envelopes. This allows the designer to formally respect the Eurocode 8 prescriptions in those countries where they also represent legal prescriptions.

The paper is organized as follows. A review of the seismic envelopes definition is summarized in Section 2 while the closed form computation of the algorithmic rotational spectra is reported in Section 3. Details about response spectrum analysis, inclusive of the algorithmic rotational spectrum, are reported in Section 4. Efficiency and limitations of the proposed strategy are discussed by numerical applications provided in Section 5 where a detailed focus is committed to the case of torsion–flexible structures. In particular, in order to present an Eurocode 8–oriented procedure, the numerical results are provided by means of the most common capacity checks prescribed by the code, such as the case of axial force – biaxial bending of RC frames, biaxial shear and biaxial inter story drifts.

Finally, future research directions are debated in the conclusions reported in Section 6.

2. Multiple response analysis by Seismic Envelopes

The classical formulation of the response spectrum analysis, such as the procedure based on the CQC combination rule [42] for combining modal responses and a subsequent SRSS combination of the outcomes of orthogonal excitations [12], computes the peaks of a single structural response. On the contrary, capacity checks often require to consider the mutual correlation between different responses, such as in the case of axial force – biaxial bending or interstory drift checks, in which at least two displacement components are combined. In all these cases, maximum values of all response components, computed by response spectrum analysis, are not synchronous.

To address multiple responses, [28, 29] introduced the concept of Seismic Envelopes which are capable of providing an interaction domain taking into account the mutual correlation of multiple responses and all possible seismic input directions. Such an approach has been implemented by [36] in a capacity check procedure for reinforced concrete frames based on the fiber-free approach [24, 22, 23].

Despite of its efficiency, the chance of performing exhaustive Eurocode 8–compliant capacity checks is compromised by the accidental eccentricity provision.

For the reader's convenience, the present section summarizes the formulation of the seismic response envelope proposed by [28], presents the drawbacks concerning the account for accidental eccentricity and introduces the solution proposed by the present research.

2.1. The seismic response envelopes

Let us consider a structural model for which a modal analysis has been performed determining modal shapes ϕ_i arranged as columns of the $m \times n$ rectangular matrix $\mathbf{\Phi}$ where m is the number of degrees of freedom and n is the number of the considered modal shapes.

Furthermore, a three-component seismic excitation is introduced by means of displacement response spectrum. In general, horizontal principal components of the ground motion are not necessarily oriented along the reference axes X_b and Y_b used for defining the model geometry. On the contrary, seismic principal axes X_e and Y_e are rotated by a *seismic input angle* θ with respect to the geometric reference system. Note that, in general, the value of θ is unknown.

For convenience, response spectrum analysis is performed introducing two sets of $n \times n$ diagonal matrices $\mathbf{D}_k$ and $\mathbf{\Gamma}_k$. Index k denotes the component of the seismic action with $k = 1, 2$ corresponding to the horizontal components

and $k = 3$ to the vertical one. Elements $D_{i,i,k}$ and $\Gamma_{i,i,k} = \gamma_i^k$, belonging to the principal diagonals of these matrices denote, respectively, the values of the displacement spectrum and of the participating factor of mode i with respect to seismic component k.

Modal combination is performed by considering cross-correlation coefficients of the Complete Quadratic Combination (CQC) procedure proposed by [42]. Those are arranged in the square matrix $\mathbf{R}$ whose element $\rho_{i,j}$ represents the correlation coefficient between modes i and j.

Referring to the cited works for details, it is proved that, for a given θ, the multi–component response of a seismic event is contained within an *Elliptical Envelope* $\mathbf{f}_\theta$ defined as:

$$\mathbf{f}_\theta\left(\theta,\, \boldsymbol{\alpha}\right) = \mathbf{f}_d + \frac{\mathbf{X}_\theta \boldsymbol{\alpha}}{\left[\boldsymbol{\alpha}^T \mathbf{X}_\theta \boldsymbol{\alpha}\right]^{0.5}} \tag{1}$$

where $\mathbf{f}_d$ is the response due to static loads, $\boldsymbol{\alpha}$ is a unitary vector of the response space acting as parameter and $\mathbf{X}_\theta$ is a 3×3 square matrix given by:

$$\mathbf{X}_\theta = \mathbf{Q}^T \left[\mathbf{Z}_1 + \mathbf{Z}_2 \sin^2\left(\theta\right) + \mathbf{Z}_3 \sin\left(\theta\right) \cos\left(\theta\right)\right] \mathbf{Q} \tag{2}$$

with $\mathbf{Q}$ representing a *shape* matrix computing the seismic responses as functions of the structural degrees of freedom. To fix ideas, in the case of axial force – biaxial bending capacity checks, the response vector is defined as $[P,\, M_1,\, M_2]$, as shown in [36], where P denotes the axial force and M_1 and M_2, respectively, the bending moments around the local axes 1 and 2 of the cross section. More in general, shape matrix $\mathbf{Q}$ can be defined so that any arrangement of structural responses is represented.

Eventually, the entries of Eq. 2 are computed by:

$$\mathbf{Z}_1 = \mathbf{\Phi} \left[\sum_{k=1}^{3} \mathbf{\Gamma}_k \mathbf{D}_k \mathbf{R} \mathbf{D}_k^T \mathbf{\Gamma}_k^T\right] \mathbf{\Phi}^T \tag{3}$$

$$\mathbf{Z}_2 = \mathbf{\Phi} \left[-\sum_{k=1}^{2} \sum_{l=1}^{2} \left(-1\right) k + l \mathbf{\Gamma}_l \mathbf{D}_k \mathbf{R} \mathbf{D}_k^T \mathbf{\Gamma}_l^T\right] \mathbf{\Phi}^T \tag{4}$$

$$\mathbf{Z}_3 = \mathbf{\Phi} \left[\sum_{k=1}^{2} \left(-1\right)^k \mathbf{\Gamma}_1 \mathbf{D}_k \mathbf{R} \mathbf{D}_k^T \mathbf{\Gamma}_2^T + \mathbf{\Gamma}_2 \mathbf{D}_k \mathbf{R} \mathbf{D}_k^T \mathbf{\Gamma}_1^T\right] \mathbf{\Phi}^T \tag{5}$$

Note that, if $\theta = 0$ and matrix $\mathbf{Q}$ is defined for a single-component response, Equation (1) computes the classic CQC + SRSS outcome considered by Eurocode 8 provisions.

In order to characterize a seismic response not depending by θ, the *Supreme Envelope* is defined by:

$$\mathbf{f}(\boldsymbol{\alpha}) = \mathbf{f}_d + \frac{\mathbf{X}_S \boldsymbol{\alpha}}{\left[\boldsymbol{\alpha}^T \mathbf{X}_S(\boldsymbol{\alpha})\,\boldsymbol{\alpha}\right]^{0.5}} \tag{6}$$

which is formally similar to Eq. (1) although its entries are computed by:

$$\mathbf{X}_S(\boldsymbol{\alpha}) = \mathbf{Q}^T \left[\mathbf{Z}_1 + \frac{1}{2}\mathbf{Z}_2 - \frac{1}{2}\mathbf{Z}_2 P_2(\boldsymbol{\alpha}) + \frac{1}{2}\mathbf{Z}_3 P_3(\boldsymbol{\alpha})\right] \mathbf{Q} \tag{7}$$

with:

$$P_2(\boldsymbol{\alpha}) = -\frac{\boldsymbol{\alpha}^T \mathbf{Q}^T \mathbf{Z}_2 \mathbf{Q} \boldsymbol{\alpha}}{H(\boldsymbol{\alpha})}; \quad P_3(\boldsymbol{\alpha}) = \frac{\boldsymbol{\alpha}^T \mathbf{Q}^T \mathbf{Z}_3 \mathbf{Q} \boldsymbol{\alpha}}{H(\boldsymbol{\alpha})} \tag{8}$$

$$H(\boldsymbol{\alpha}) = \left[\left(\boldsymbol{\alpha}^T \mathbf{Q}^T \mathbf{Z}_2 \mathbf{Q} \boldsymbol{\alpha}\right)^2 + \left(\boldsymbol{\alpha}^T \mathbf{Q}^T \mathbf{Z}_3 \mathbf{Q} \boldsymbol{\alpha}\right)^2\right]^{0.5} \tag{9}$$

Equations (6)–(9) have been derived by maximizing the response of Eq. (1) with respect to θ; thus, the Supreme Envelope contains all the elliptical envelopes computed by spanning the value of θ between 0 and 2π.

It is worth to be emphasized that the Supreme Envelope represents an extension of the CQC3 modal combination rule [38] to multiple–component responses. Further details of the definitions of the quantities introduced in the present section are omitted for brevity and are reported by [28]. Nonetheless, the supreme envelope is a compact domain, defined in the seismic response space, which encompasses all the possible structural responses due to a multi–component seismic load, for all the possible orientations of the earthquake input directions.

2.2. Use of seismic envelopes in presence of accidental eccentricity and global torsion

In order to fulfill the Eurocode 8 provisions, the accidental eccentricity has to be introduced. In such a case, the use of Supreme Envelope of Eqs. (3)–(9) is compromised by the requirement of shifting the mass from its original position. To fix ideas, the peak responses due to a seismic action $\mathbf{D}_1$ acting along axis X_b should be computed by shifting the structural mass of an eccentricity $\pm e_1$ corresponding to locations N and S in Fig. 1(a). Moreover, seismic responses

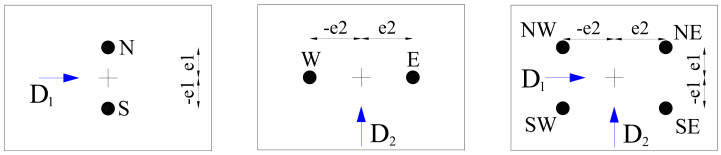

(a) Mass locations for $\mathbf{D}_1$ seismic actions

(b) Mass locations for $\mathbf{D}_2$ seismic actions

(c) Combined mass locations

Figure 1: Mass locations relevant to different seismic input actions

due to the action $\mathbf{D}_2$ acting along axis Y_b should assume an eccentricity of $\pm e_2$ corresponding to locations E and W in Fig. 1(b).

It must be emphasized that mass shifting of Figs. 1(a) and 1(b) correspond to four different structural models, each one with their own modal shapes. For this reason, it is not possible to define a single modal shape matrix $\mathbf{\Phi}$ to be used in Eqs. (3)–(5) so that four separate structural models should be considered to evaluate seismic envelopes.

A possible solution consists in considering the mass locations reported in Figure 1(c); nevertheless, such a strategy provides approximate results since it does not fulfill the theoretical formulation of the Supreme Envelope. In fact, the points belonging to the envelope boundary represent the maximum seismic response due to any possible direction of the ground motion so that such an envelope accounts for an infinite number of orientations of the seismic input axes. Therefore, considering that structural masses are shifted by the accidental eccentricity along the direction orthogonal to the seismic axes, the structural model should account for an infinite number of mass locations. Moreover, although locations represented in Figure 1(c) can be assumed as a reasonable approximation, the presence of four structural models requires to perform four capacity check procedures at each cross section of interest making the structural design computationally demanding.

An effective approach to account for global torsion in buildings, alternative to the accidental eccentricity, consists in including a further response spectrum relevant to the rotational component, about axis Z_e, of the ground motion. This makes the computation of the Supreme Envelope straightforward and computationally efficient since, assuming the global torsion seismic component to be uncorrelated from the remaining ones, the only modification in computing the elliptical and supreme envelopes consists in introducing a further term in Eq. 3 which is up-

dated as:

$$\mathbf{Z}_1 = \mathbf{\Phi} \left[\mathbf{\Gamma}_\theta \mathbf{D}_\theta \mathbf{R} \mathbf{D}_\theta^T \mathbf{\Gamma}_\theta^T + \sum_{k=1}^{3} \mathbf{\Gamma}_k \mathbf{D}_k \mathbf{R} \mathbf{D}_k^T \mathbf{\Gamma}_k^T \right] \mathbf{\Phi}^T \tag{10}$$

where $\mathbf{D}_\theta$ are the modal values of the torsional response spectrum and $\mathbf{\Gamma}_\theta$ are the relevant participation factors.

From a computational point of view, the introduction of a further matrix product is a sensibly irrelevant effort for an analysis algorithm with respect to three further modal analyses involving control flows about the location of the structural masses.

3. Algorithmic rotational spectrum

The procedure proposed in this paper aims to include the rotational spectrum formulation, in the ordinary response spectrum analysis, by replacing the prescribed accidental eccentricity with an algorithmic response spectrum characterizing a fictitious rotational ground motion acting about axis $Z_e \equiv Z_b$. For the sake of simplicity but without limiting the generality of the approach, we assume the origin of the global reference on the vertical alignment of the global center of mass of the structure, i.e., the point whose coordinates $[x_g\, y_g\, z_g]$ in a generic reference system are:

$$\begin{bmatrix} x_g \\ y_g \\ z_g \end{bmatrix} = \sum_{i=1}^{n} \begin{bmatrix} x_i m_i \\ y_i m_i \\ z_i m_i \end{bmatrix} \frac{1}{\sum_{i=1}^{n} m_i} \tag{11}$$

where m_i is the mass of the ith structural node and $[x_i\, y_i\, z_i]$ are the relevant coordinates.

Let us model the rotational components of the earthquake action as a rigid rotation of the base floor. Thus, given a rotational acceleration $a_{\theta z}$, a generic point with coordinates $(\bar{x}, \bar{y})$ would be subjected to an acceleration with components:

$$\mathbf{a}\,(\bar{x}, \bar{y}) = \begin{bmatrix} -\bar{y} a_{\theta z} & \bar{x} a_{\theta z} & 0 & a_{\theta z} \end{bmatrix} \tag{12}$$

Let D_1, D_2 and D_3 be the design displacement–response spectra of the translational DOFs computed by the corresponding pseudo–acceleration response spectra S_1, S_2 and S_3. The proposed algorithm consists in:

1. evaluating dynamic properties of the structural model, i.e., modal frequencies ω_i and shapes ϕ_i by means of a modal analysis;

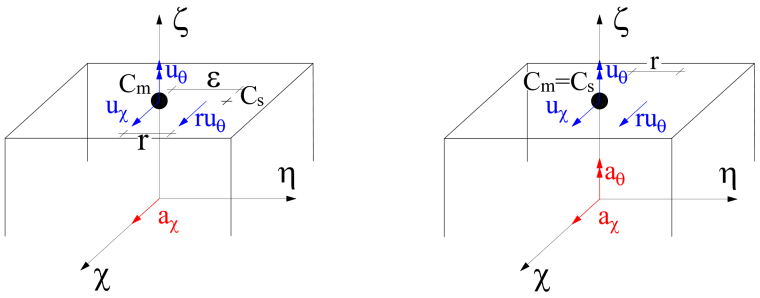

(a) Coupled Oscillator (b) Uncoupled Oscillator

Figure 2: Idealized 2–DOFs oscillators

2. introducing an algorithmic rotational response spectrum, D_θ, depending on both translational spectra and dynamic properties of the structure, as detailed in the following subsections;

3. Determining the seismic response by means of the elliptical or supreme envelope of Eqs. (1) and (6), accounting for the rotational spectrum by Eq. (10).

Because of the mandatory nature of some code provisions, such as [14] and [32], the rotational spectrum cannot be chosen among the formulations provided by the literature despite of their theoretical correctness. On the contrary, it is necessary to introduce a suitable definition of the rotational spectrum that makes it equivalent to the accidental eccentricity provision and, at the same time, provides equal or conservative responses.

To fulfill this last condition, the theoretical definition of an algorithmic rotational spectrum D_θ, specifically developed in this research, is presented in Subsection 3.1 together with the derivation of its closed form expression.

Moreover, an alternative algorithmic rotational spectrum is derived in order to compare the seismic responses provided by the proposed spectrum with similar formulations. Specifically, Subsection 3.2 introduces an algorithmic spectrum derived by inverting the accidental eccentricity provision proposed by [3].

3.1. Formulation of the Dynamic–Equivalent Rotational Spectrum (DERS)

To define the algorithmic rotational spectrum, the dynamic behavior of the whole structure is hereby modeled by means of single–story equivalent oscillators. Such an equivalence, although approximated, has already been exploited

in the literature in order to check the suitability of code accidental eccentricity prescription with respect to real rotational motions [9, 10].

In particular, in order to compare the dynamic behavior of structures with several degrees of freedom by means of a single response, coupled and uncoupled single–story oscillators were defined by [9]. Equivalence between their responses was defined in terms of the normalized displacement at a fixed point in order to check if the coupled oscillator provided the same responses as the corresponding one of the uncoupled oscillator subject to a recorded rotational action.

Conversely, the proposed approach aims to follow the inverse path since the eccentricity is provided by the code provisions and a fictitious rotational spectrum able to produce the given eccentricity is looked for.

Equivalent oscillators, depicted in Figures 2(a) and 2(b), consist of a rigid diaphragm with mass lumped at C_m and static forces applied at C_s. Both oscillators are defined in an auxiliary three–dimensional space with axes χ, η and ζ and characterized by the eccentricity ε and radius of gyration r about axis ζ.

The degrees of freedom governing the structural motions are the horizontal displacement u_χ and the rotation u_θ about axis ζ at the center of mass. The systems are subject to an acceleration $a_\chi(t)$ acting along the horizontal direction χ and a rotational acceleration $a_\theta(t)$ acting about the vertical axis ζ. The *coupled* oscillator is defined in order to provide a response which is representative of the structure subject to the accidental eccentricity prescribed by structural codes while the *uncoupled* one aims to be representative of the structure with no eccentricity, subject to the algorithmic rotational spectrum to be determined.

The structural behavior of both oscillators is characterized by means of natural frequencies, specifically, the lateral frequency $\omega = 2\pi/T$ and the rotational one $\omega_\theta = \omega\Omega = 2\pi\Omega/T$, T being the natural period and $\Omega = \omega_\theta/\omega$ the frequency ratio introduced by [39]. Both ω and Ω are evaluated by the results of the modal analysis, as illustrated in Section 4, in order to make the oscillator representative of a real structural model.

The *coupled* oscillator, depicted in Figure 2(a) is characterized by a prescribed eccentricity ε and it is subject to a translational motion by means of the design displacement response spectrum $D_\chi(T)$.

At the present stage, the value of ε is assumed to be a fixed value defined by the designer or by code provisions; further details on this issue will be provided in Section 4.2.

The *uncoupled* oscillator is characterized by zero eccentricity and it is subject to lateral and rotational motion $D_\chi(T)$ and $D_\theta(T/\Omega)$, respectively. While response spectrum $D_\chi(T)$ is defined by the designer, the rotational spectrum

$D_\theta(T/\Omega)$ is evaluated by imposing equivalence between the coupled and uncoupled oscillator in terms of the peak displacement u_θ, i.e., the rotation about ζ at the center of mass.

Summarizing, the definition of the algorithmic rotational spectrum is the following:

Definition 1. *Provided a single–story oscillator with natural frequency $\omega = 2\pi/T$, radius of gyration r and frequency ratio Ω, the quantity $D_\theta(T/\Omega)$ is the rotational spectrum intensity that produces the same rotation about vertical axis ζ that would be computed in the case of accidental eccentricity ε.* □

To determine a closed–form expression of D, the equivalent oscillators responses are computed by their equation of motion. In particular, the response of the oscillators depicted in Figure 2 is ruled by:

$$\begin{bmatrix} \ddot{u}_\chi \\ r\ddot{u}_\theta \end{bmatrix} + \begin{bmatrix} \omega^2 & \dfrac{\omega^2\varepsilon}{r} \\ \dfrac{\omega^2\varepsilon}{r} & \omega^2\Omega^2 + \dfrac{\varepsilon^2}{r^2} \end{bmatrix} \begin{bmatrix} u_\chi \\ ru_\theta \end{bmatrix} = - \begin{bmatrix} a_\chi(t) \\ ra_\theta(t) \end{bmatrix} \tag{13}$$

where, in order to express displacements homogeneously, rotation u_θ has been replaced by ru_θ, i.e., the displacement along χ, associated only with the rotation u_θ, of the point at distance r from the center of mass.

The equation of motion (13) formally applies to both oscillators which are characterized by the acceleration components defined in Table 1.

Table 1: Acceleration components of coupled and uncoupled oscillators

Oscillator	ε	a_x	a_θ
Coupled	ε code prescribed	$a_\chi \to D_\chi(T)$	$a_\theta = 0$
Uncoupled	$\varepsilon = 0$	$a_\chi \to D_\chi(T)$	$a_\theta \to D_\theta(T/\Omega)$

Equation (13) is solved in order to compute the rotational response spectrum $D_\theta(T/\Omega)$ so as to guarantee equal values of the peak displacements ru_θ for both oscillators.

In case of $\varepsilon = 0$, matrix governing Eq. (13) is diagonal so that the uncoupled oscillator acts as the superposition of two independent single-degree of freedom

(SDOF) oscillators. Thus, the peak value of the displacement ru_θ of the uncoupled oscillator is trivially:

$$\max\left[ru_\theta\left(t\right)\right] = rD_\theta\left(T/\Omega\right) \tag{14}$$

while the analogous peak rotational displacement of the coupled oscillator can be computed by a standard response spectrum analysis. In particular, as shown in Appendix AppendixA, the periods T_1 and T_2 of the two modal shapes turn out to be:

$$T_1 = \frac{2\pi}{\sqrt{c-R}}; \quad T_2 = \frac{2\pi}{\sqrt{c+R}} \tag{15}$$

where:

$$c = \omega^2\frac{1+\Omega^2+\varepsilon^2/r^2}{2}; \quad R = \frac{\omega^2}{2}\sqrt{\left(\Omega^2+\varepsilon^2/r^2-1\right)^2+4\varepsilon^2/r^2} \tag{16}$$

Denoting by $D_{\chi,1}$ and $D_{\chi,2}$ the relevant values of the displacement response spectrum of the translational ground motion, the peak response is computed by the well established CQC superposition rule [38] with correlation coefficient:

$$\rho_{1,2} = \frac{8\xi^2\left(T_2/T_1\right)^{3/2}}{\left(1+T_2/T_1\right)\left[\left(1-T_2/T_1\right)^2+4\xi^2\left(T_2/T_1\right)\right]} \tag{17}$$

where ξ is the damping coefficient, supposed to be the same for both modes. Therefore, the peak value of the response ru_θ due to the rotation only is:

$$\max\left(ru_\theta\right) = \frac{c_1c_2}{c_1+c_2}\sqrt{D_{\chi,1}^2+D_{\chi,2}^2-D_{\chi,1}D_{\chi,2}\rho_{1,2}} \tag{18}$$

where c_1 and c_2 have been defined as:

$$c_1 = \left(\omega^2\varepsilon/r\right)^2; \quad c_2 = \left(-\omega^2+c-R\right)^2 \tag{19}$$

Enforcing the equivalence between responses (14) and (18), the rotational response spectrum providing the same maximum displacement of the uncoupled oscillator as the coupled one is:

$$D_\theta\left(T/\Omega\right) = \frac{\max\left(ru_\theta\right)}{r} = \frac{c_1c_2}{r\left[c_1+c_2\right]}\sqrt{D_{\chi,1}^2+D_{\chi,2}^2-D_{\chi,1}D_{\chi,2}\rho_{1,2}} \tag{20}$$

while the corresponding pseudo–acceleration and pseudo–velocity spectra are:

$$S_{a\theta,\chi}\left(S_\chi,T\right) = D_\theta\left(T/\Omega\right)\omega^2; \quad S_{v\theta,\chi}\left(S_\chi,T\right) = D_\theta\left(T/\Omega\right)\omega \tag{21}$$

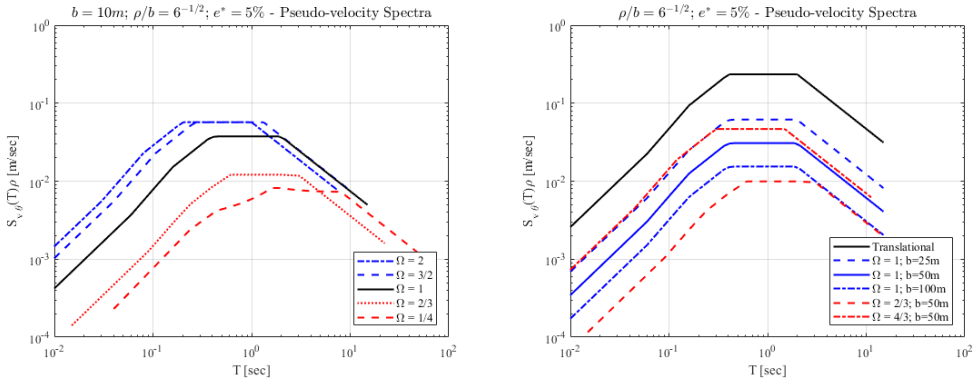

(a) Ω variable (b) b variable

Figure 3: Global torsion response spectra

Examples of rotational pseudo–velocity spectra defined by Equation (21) are plotted in Figure 3, together with the corresponding translational spectrum, where b represents the maximum horizontal dimension of the structure. Specifically, algorithmic spectra plotted in Figure 3(a) have been computed with $b = 10m$, accidental eccentricity $\varepsilon = 0.05b = 0.5m$, radius of gyration $r = b/\sqrt{6}$ and considering several values of $\Omega = \omega_\theta/\omega$. The black solid line corresponds to $\Omega = 1$, i.e. the rotational frequency is equal to the translational one. The plot shows that response spectra peaks increase in value and are attained for lower periods T as Ω increases.

In Figure 3(b) plots of Pseudo–velocity spectra are plotted for different vaues of b. It is shown how the spectra increases proportionally to the value of b.

The plotted algorithmic spectra can be sensibly different if compared with recorded or theoretically derived ones. In this respect we emphasize once more that the algorithmic rotational spectrum does not aim to physically characterizing ground motions since its objective is to model the contribution of geometrical phenomena by means of a spectral interpretation. In fact, as previously stated, its purpose is to apply a code prescription which is not necessarily consistent with the real rotational component of any real ground motion. Nevertheless, we emphasize that the shape of the pseudo-velocity response spectra, presenting three almost-linear branches in the logaritmic space, turns out to be consistent with the shape derived by [31] and [9].

3.2. Formulation of the Static–Equivalent Rotational Spectrum (SERS)

Investigations concerning accidental torsion presented by [3] propose a formulation of the accidental eccentricity in order to reproduce the effects of rotational ground motions. Such an approach is the sole, among all the strategies reported in Section 1, to establish a direct relationship between accidental eccentricity and the rotational spectrum. For this reason, it is hereby summarized and extended to response spectrum analysis in order to provide a comparison benchmark for the rotational spectrum introduced in Subsection 3.1.

Specifically, the procedure presented by [3] takes into account rotational effects of a translational time series by introducing an artificial rotational motion which replaces the shifting of the center of mass due to the accidental eccentricity. An equivalence, similar to the one presented in Subsection 3.1, is enforced between two structural systems in terms of inertial forces. In particular, the first system, presenting an accidental eccentricity ε_a, is subject to a translational ground motion while the second one, with zero eccentricity, is subject to both a translational ground motion and the artificial rotational one.

This latter turns out to be easily computed as function of the translational one; in particular, it is stated in Section 4 of [3]:

"The equivalent ground motion consists of the original translational motion and a rotational motion calculated by multiplying the translational motion by an "arm" ε_a/r^2".

Consequently, substituting the times series of the ground motion by its translational response spectrum D_u the artificial rotational spectrum $D_\theta(T)$ is defined by [3] as:

$$D_\theta(T) = D_u(T)\,\frac{\varepsilon_a}{r^2} \tag{22}$$

where r represents the radius of inertia and ε_a the accidental eccentricity.

It is worth to be emphasized that, unlikely most of the investigations about global torsion, see, e.g., [10, 9] which make an explicit reference to the frequency ratio Ω and/or the stiffness, such an artificial spectrum is independent from the dynamical properties of the analyzed structure.

Considering that the approach herein illustrated is based on inertial forces, the artificial rotational spectrum defined in Equation (22) will be addressed in the sequel as Static Equivalent Rotational Spectrum (SERS).

4. Eurocode 8 – compliant seismic analysis based on the algorithmic rotational spectrum

In order to exploit the features of the algorithmic rotational spectrum defined in the previous section and illustrate its application, the proposed strategy for structural seismic analysis requires the definition of a fully–3D structural model where no accidental eccentricity has been applied. A classic modal analysis is first performed in order to obtain modal shapes $\bar{\phi}_i$, natural frequencies ω_i, participation factors γ_i^x, γ_i^y for excitations acting along x and y, respectively, and participation factors γ_i^θ for the global torsion excitation.

The structural model with unperturbed mass is characterized by dynamic properties, such as modal periods, shapes and participating factors, different from the ones relevant to the models with shifted masses. The relevant variations mostly depend upon the mechanics of the structural model and exhibit a degree of accuracy analogous to alternative procedures based upon accidental eccentricity.

Actually, accidental eccentricity was introduced by [31] in order to account for torsional effects of a *single* structural model, meaning that the *correct* model is intended with unperturbed mass; hence, models with eccentric masses turn out to be conventional. Moreover, the use of the unperturbed model is a practice common to several computational procedures, included the torsional moment provision by [14] as well as the strategies proposed by [15], [8] and [3].

For each modal shape $\bar{\phi}_i$, response spectrum analysis usually computes seismic responses, depending on the associated response spectrum, which are subsequently combined by means of a modal combination rule. In this sense, the overall structural behavior is modeled as the superposition of several single-degree-of-freedom oscillators. In particular, recalling Definition 1 of the algorithmic rotational spectrum provided in Section 3.1, the quantity $D_\theta(T/\Omega)$ can be interpreted as the spectral intensity to be applied to an oscillator with a translational and a rotational DOFs, in order to produce the same rotation u_θ that would have been computed in the case of accidental eccentricity ε. Therefore, it is reasonable to assume that the application of the spectral intensity $D_\theta(T/\Omega)$ to each mode would generate a rotational response similar to the one produced by the accidental eccentricity.

Although this latter assumption is theoretically incorrect, the approximations introduced in this way are expected to be of the same order of magnitude of those considered by [9] where the same simplified model was used for calibrating accidental eccentricity from recorded ground motions.

In order to evaluate the rotational equivalent spectrum as defined in Section

3 further quantities need to be defined: the frequency ratio Ω, the radius of gyration r and the accidental eccentricity ε. In the case of structures with multiple degrees of freedom, their definition is not straightforward as for the single–story oscillator. Specifically, the value of the accidental eccentricity depends upon the input direction of the ground motion which is not known in advance; furthermore, whenever the structure presents more than two modal shapes, the frequency ratio Ω is not univocally defined.

4.1. Structural frequency ratio Ω

The frequency ratio Ω has been defined in Section 3 for two DOFs structural models as the ratio ω_θ/ω between the rotational and lateral frequency. Extension of this definition to multi–story buildings can be done only on a conventional basis.

The procedure presented by [20] defines Ω by means of the dominant translational and rotational modes, i.e. the ones characterized by the maximum values of γ_i^x, γ_i^y and γ_i^θ, respectively. Denoting by $\omega_{k_{tr}}$ the natural frequency corresponding to the modal shape with the maximum participation factor among γ_i^x and γ_i^y, and by ω_{k_θ} the natural frequency associated with the maximum γ_i^θ, the value of Ω to be used for the application of the algorithmic rotational spectrum is assumed to be:

$$\Omega = \frac{\omega_{k_\theta}}{\omega_{k_{tr}}} = \frac{T}{T_\theta} \tag{23}$$

As pointed out by [2], the frequency ratio (23) is not univocally defined since ω_{k_θ} depends upon the polar moment of inertia which, in turn, depends upon the global reference system. Nevertheless, formulation of Eq. (23) is the most reasonable one to be adopted in code – compliant analyses since it is employed by standard codes such as the Uniform Building Code [17] and the Annex A of the [14].

4.2. Radius of gyration r and accidental eccentricity ε

An additional quantity which needs to be properly defined for extending the algorithmic rotational spectrum to multi–story buildings is the radius of gyration r. Its definition is straightforward since we can set $r = \sqrt{I_z/m_{tot}}$ where m_{tot} denotes the total mass of the building and I_z is the polar moment of inertia of the building about the z–axis computed as sum of the polar moment of inertia I_{iz} of the i–th floor.

Finally, to apply the algorithmic rotational spectrum we need to define the accidental eccentricity ε. Several design codes define ε as a percentage of the plan size of the building b perpendicular to the direction of ground motion. However, such a definition implies that the direction of the seismic excitation is known or arbitrarily fixed while use of supreme envelope implies that seismic input direction spans all the horizontal plan. For this reason, the designer should define the value of the accidental eccentricity depending on the features of the analyzed model and on its experience. Postponing to future publications more specific investigations, a conservative choice is to define b as the maximum horizontal distance between two nodes of the base floor of the building.

4.3. Modal superposition and seismic responses

Once the frequency ratio, the radius of gyration and the accidental eccentricity have been defined, the rotational spectrum is computed by the procedure described in Subsection 3.1. In particular, the displacements response spectra modal values D_i^k correspond to the translational seismic components along x and y for $k = 1$ and $k = 2$, respectively, to the translational component along axis z for $k = 3$ and to the rotational spectrum for $k = 4$.

Matrices $\mathbf{Z}_1$, $\mathbf{Z}_2$ and $\mathbf{Z}_3$ are computed by equations (10), (4), (5), respectively, and seismic responses are finally computed either by the supreme envelope (Eqs. (6)–(9)) or by the elliptical one (Eqs. (1) and 2) both performing the CQC3 modal combination.

In this respect we emphasize that such a superposition implicitly considers the rotational spectrum as statistically independent from the translational ones. Although numerical evidences provided in the following subsections seem to support such an assumption, this undoubtedly represents a topic of further investigation.

5. Numerical applications

The strategy presented in Section 3 has been applied to four linear structural models illustrated in Figures 4 and 5. The first two structures, denoted as building A and B respectively, are 3D six–story reinforced concrete frames symmetrical in plan. Although similar, these two models are representative of a rotationally stiff frame (building A, Figure 4(a)) and a rotationally flexible structure (building B, Figure 4(b)).

Moreover, two further models, denoted as building C and D in Fig. 5, present structural irregularities. Specifically, building C is a six–story reinforced concrete frame with irregular plan illustrated in Figure 5(a) and elevation in Figure 5(c)

while Building D, whose elevation is represented in Figure 5(d), has irregularities both in plan and in elevation. In particular, stories 1–3 have the same plan as building C (see Figure 5(a)) while the plans of stories 4–6 of building D are represented in Figure 5(b).

All buildings have interstory height equal to $3.0\,m$ and rigid diaphragm at each floor with uniformly distributed translational mass along x and y equal to $750\,Kg/m^2$. The floor masses and polar moments of inertia are applied at the geometrical centers of each floor. Global reference axes have been located on the vertical alignment of the global centers of mass of the structures.

Base nodes have been assumed completely fixed while beams and columns have different cross sections. Specifically, buildings A, C and D have concrete beams with $0.3 \times 0.6\,m$ rectangular cross section. Columns vary along the height: $0.3 \times 0.7\,m$ at the first two stories, $0.3 \times 0.5\,m$ at 3rd and 4th story and $0.3 \times 0.3\,m$ at 5th and 6th ones. Building B presents concrete beams with 0.3×0.6 square cross section, steel columns with HEB200 cross section and a square–pipe–shaped concrete kernel of width of $3.0\,m$ and thickness $0.5\,m$.

Reinforcement bars in RC sections has been arranged at their corners, each bar having area equal to 1% of the concrete area. Stirrups have been assumed to be two–braces, rectangular–shaped uniformly distributed along all structural members, having $\phi 8$ mm diameter and 0.1 m spacing. Young modulus is equal to $E_c = 27600$ MPa for concrete members and to $E_s = 220000$ MPa for steel members.

The radius of gyration for structural models A, C and D has been computed, on the basis of the assumptions of Sections 4.1 and 4.2, by supposing the floor masses uniformly distributed on the floor plan while for building B, in order to obtain a small frequency ratio Ω, a radius of gyration $r = 8.96\,m$ has been assumed. Such a value has been computed by considering a non–uniform mass distribution accounting for the presence of external walls at the edge of the structure.

Frequency ratios have been computed by Equation (23) where T is the period of the main "lateral" mode while T_θ is the period of the main rotational one. Specifically, main modes are defined as the ones corresponding to the highest participation factors for the translational and rotational seismic components, respectively. The numerical value of all dynamic parameters are summarized in Table 2 where periods of the main translational and rotational modal shapes, T and T_θ are also reported.

According to the Eurocode 8, the accidental eccentricity has been set at the 5% of the planar dimension orthogonal to the seismic input direction. It is worth being emphasized that, in the case of responses computed by the supreme envelope,

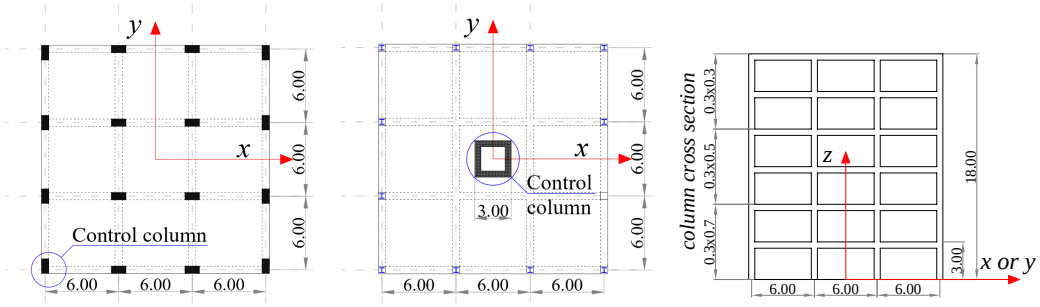

(a) Building A: Rotationally stiff

(b) Building B: Rotationally flexible

(c) Buildings A and B elevation

Figure 4: Buildings A and B structural frames

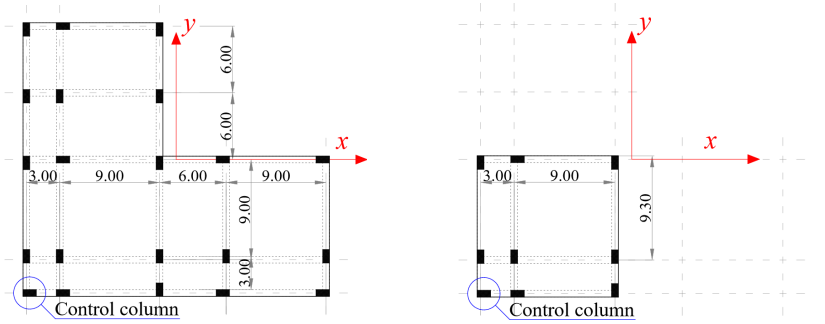

(a) Plan for building C and for floors 1-3 of building D

(b) Building D plan (floors 4–6)

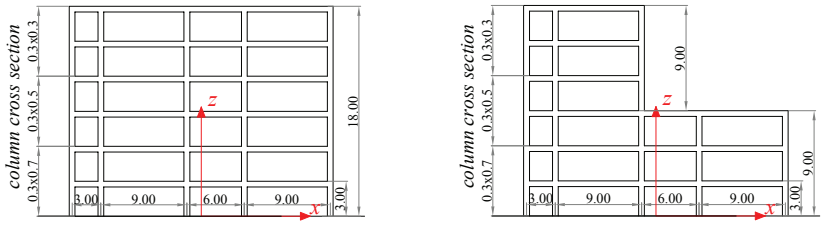

(c) Building C elevation

(d) Building D elevation

Figure 5: Buildings C and D structural frames

Table 2: Dynamic properties of buildings A–D

Building	r [m]	ε [m]	T [sec]	T_θ [sec]	Ω
A	7.35	1.30	1.19	0.88	1.40
B	8.96	1.30	0.74	0.71	1.04
C	9.00	1.81	1.18	0.76	1.55
D	9.00	1.81	0.92	0.31	3.00

being seismic input directions not fixed, the planar dimension of the building has been assumed equal to the larger diagonal of the structural plan as specified in Section 4.2.

The vertical ground motion (i.e. translation along z) has been omitted in the present comparison because it does not interact with accidental eccentricity. Should the vertical seismic component be needed in structural analysis, its response can be simply combined as in Eq. (10).

Vertical loads have been assigned by means of simply supported decks aligned along the global y axis with load $750{\cdot}9.81\ N/m^2$ resulting in uniformly distributed loads applied to the beams aligned along the global x axis.

In order to get a significant comparison of the results provided by the proposed method with respect to alternative strategies, the response spectrum analysis of the considered buildings has been performed and the structural responses, computed by means of seismic envelopes, have been used in capacity check operations. In particular, three typologies of check have been considered:

1. Serviceability Limit State based on thresholds of the Interstory Drift;
2. Ultimate Limit State based on the concrete shear capacity of the cross sections;
3. Ultimate Limit State based on the axial force - biaxial bending capacity of the cross sections.

Such capacity check typologies have been selected in order to be consistent with the most popular procedures for structural design adopted in common practice and recommended by code provisions.

5.1. Serviceability Limit State capacity check

The serviceability limit state is performed by computing the interstory drift, defined as maximum relative horizontal displacement between two consecutive,

vertically aligned nodes. The limit state condition is defined by means of a threshold interstory drift assumed to be $u^\star = 0.005 \cdot 3.00\, m = 0.0015\, m$, i.e., the 0.5% of the interstory height.

In order to numerically characterize such a limit state condition, we consider the generic node $P(x, y, z_j)$ belonging to floor j located in plan at (x, y). The corresponding drift vector $\Delta\mathbf{u}_j\,(x, y, \alpha)$ is computed by means of supreme envelope.

To this end, it is necessary to define the shape matrix $\mathbf{Q}_u$ in order to compute Equations (3)–(9). Recalling that the considered structural models present rigid diaphragms at all floors, interstory drifts can be computed as linear combination of all displacement components. In particulat, matrix $\mathbf{Q}_u$ has to be defined so that the product $\mathbf{Q}_u^T\mathbf{\Phi}$ yields:

$$\mathbf{Q}_u^T\mathbf{\Phi} = \begin{bmatrix} \Delta u_{x,j}^1 & \dots & \Delta u_{x,j}^i & \dots & \Delta u_{x,j}^n \\ \Delta u_{y,j}^1 & \dots & \Delta u_{y,j}^i & \dots & \Delta u_{y,j}^n \end{bmatrix} \tag{24}$$

where $\Delta u_{x,1}^i$ and $\Delta u_{y,1}^i$ are the components of the j-th interstory drift relevant to modal shape $i \leq n$. Using matrix $\mathbf{Q}_u$ in Equations (4)–(9), the supreme envelope of Eq. (6) computes the interstory drift $\Delta\mathbf{u}_j\,(x, y, \alpha)$.

At each point (x, y), the serviceability limit condition is defined as a circle of equation:

$$\|\Delta\mathbf{u}_j\,(x, y, \alpha)\| \leq u^\star \tag{25}$$

and it is equivalent to check that the critical multiplier $\lambda_{u,j}$ is greater than or equal to 1:

$$\lambda_{u,j} = \max_{x,y,\alpha}\left[\frac{\|\Delta\mathbf{u}_j\,(x, y, \alpha)\|}{u^\star}\right] \geq 1 \tag{26}$$

Notice that the maximum critical multiplier $\lambda_{u,j}$ of the j-th interstory drift is computed at the points located at the corners of the building plan. Physically, multiplier $\lambda_{u,j}$ is the scalar which amplifies the response spectra of the seismic loads so as to make the supreme envelope tangent to the limit state circle defined in Equation (25).

5.2. Shear Ultimate Limit State capacity check

Capacity checks relevant to the shear ultimate limit state are performed by computing, by the supreme envelope, a seismic response consisting in the two shear components V_1 and V_2. In particular, this is done by conveniently defining a shape matrix $\mathbf{Q}_s$ so that the product with the modal shape matrix $\mathbf{\Phi}$ yields a matrix whose columns are the shear components corresponding to each modal shape:

$$\mathbf{Q}_s^T\mathbf{\Phi} = \begin{bmatrix} V_{1,j}^1 & \dots & V_{1,j}^i & \dots & V_{1,j}^n \\ V_{2,j}^1 & \dots & V_{2,j}^i & \dots & V_{2,j}^n \end{bmatrix} \tag{27}$$

where index j denotes the j-th cross section at which the shear capacity check is performed and index $i \leq n$ is relevant to the i-th modal shape. Using matrix $\mathbf{Q}_s$ in Equations (4)–(9), the supreme envelope computed by Eq. (6) yields the shear vector $[V_{1,j}(\boldsymbol{\alpha})\ V_{2,j}(\boldsymbol{\alpha})]^T$ of the j-th cross section.

The Ultimate Limit State function relevant to the shear collapse is defined by means of the relationship provided by [13] in which ultimate limit values of the shear are defined as:

$$V_{U,1} = \min\left[V_{Rd2,1},\, V_{Rd3,1}\right]; \quad V_{U,2} = \min\left[V_{Rd2,2},\, V_{Rd3,2}\right] \tag{28}$$

where $V_{U,1}$ and $V_{U,2}$ denote the ultimate shear values for axes 1 and 2 of the cross section, respectively. The quantities $V_{Rd2,1}$ and $V_{Rd2,2}$ denote the shear ultimate value due to the collapse of the compressed concrete diagonal:

$$V_{Rd2,1} = \frac{0.9\,\nu f_{cd} b_{w,1} l_1^\star}{2}; \quad V_{Rd2,2} = \frac{0.9\,\nu f_{cd} b_{w,2} l_2^\star}{2}; \tag{29}$$

in which f_{cd} is the concrete design strength, $b_{w,1}$ and $b_{w,2}$ are the dimensions of the cross section normal to shear components 1 and 2, respectively, $l_1^\star$ and $l_2^\star$ effective dimension of the cross section parallel to shear components and $\nu = 0.7 - f_{ck}/200$ is an efficiency coefficient. Furthermore, $V_{Rd3,1}$ and $V_{Rd3,2}$ represent the shear ultimate values corresponding to the yield of stirrups:

$$V_{Rd3,1} = \frac{0.9 l_1 \mu_{s1}}{i_s} f_y; \quad V_{Rd3,2} = \frac{0.9 l_2 \mu_{s2}}{i_s} f_y \tag{30}$$

where l_1 and l_2 are the dimensions of the considered cross section along local directions 1 and 2, respectively; μ_{s1} and μ_{s2} are the values of the cross area of stirrup braces aligned along local directions 1 and 2, respectively, i_s is the longitudinal spacing between stirrups and f_y is their strength.

The limit state condition is defined by means of an elliptical capacity domain with semi-axes V_{U1} and V_{U2}:

$$\frac{1}{\lambda_{s,j}^2} = \left[\frac{V_{1,j}(\boldsymbol{\alpha})}{V_{U1}}\right]^2 + \left[\frac{V_{2,j}(\boldsymbol{\alpha})}{V_{U2}}\right]^2 \leq 1 \tag{31}$$

In this case, the value of the critical multiplier $\lambda_{s,j}$, i.e. the scalar which, multiplied by the response spectra of the seismic excitation, makes the shear supreme envelope of cross section j be tangent to the shear capacity domain, turns out to be the square root of the reciprocal of the ultimate limit function.

5.3. Axial force – Biaxial bending Ultimate Limit State capacity check

Axial force - biaxial bending ultimate limit state check is performed by defining the shape matrix so that the seismic response consists in a vector containing the axial force and two bending moments relevant to a specified cross section. To this end, matrix $\mathbf{Q}_b$ is defined so that it yields:

$$\mathbf{Q}_b^T \mathbf{\Phi} = \begin{bmatrix} P_j^1 & \dots & P_j^i & \dots & P_j^n \\ M_{1,j}^1 & \dots & M_{1,j}^i & \dots & M_{1,j}^n \\ M_{2,j}^1 & \dots & M_{2,j}^i & \dots & M_{2,j}^n \end{bmatrix} \tag{32}$$

where $i \leq n$ is the modal shape index, j denotes a cross section of interest, P_j^i, $M_{1,j}^i$ and $M_{1,j}^i$ denote the axial force and bending moments about local axes 1 and 2, respectively, of cross section j and mode i. Therefore, the seismic response of cross section j computed by the supreme envelope of Eq. (6) is:

$$\mathbf{f}_j(\boldsymbol{\alpha}) = \left[P_j(\boldsymbol{\alpha})\ M_{1,j}(\boldsymbol{\alpha})\ M_{1,j}(\boldsymbol{\alpha})\right]^T \tag{33}$$

The Ultimate Limit state condition for axial force - biaxial bending loads at cross section j can be expressed by the implicit function:

$$\mathcal{F}_b[\mathbf{f}_j] = 0 \tag{34}$$

in which $\mathbf{f}_j$ denotes the load vector. The locus of all vectors $\mathbf{f}_{u,j}$ fulfilling condition (34) is defined as bending capacity domain and is computed by means of a nonlinear algorithm presented by [1] and implemented in Matlab. The domain encompasses all load states assumed to be safe for the j-th cross section.

The capacity check procedure adopted in the present research consists in finding out if the supreme envelope is fully contained inside the capacity domain. In particular, computations have been carried out by the algorithm presented by [36] in which the critical multiplier $\lambda_{b,j}$, defined as:

$$\lambda_{b,j} = \arg\min_{\lambda} \left\{\exists \boldsymbol{\alpha}^\star : \mathcal{F}_b\left[\lambda\, \mathbf{f}_j(\boldsymbol{\alpha}^\star)\right] = 0\right\} \tag{35}$$

is determined as the minimum multiplier of the seismic response spectra (i.e. of load $\mathbf{f}_j(\boldsymbol{\alpha})$) for which it is possible to determine at least an outcome $\boldsymbol{\alpha}^\star$ of the unit vector $\boldsymbol{\alpha}$ fulfilling the ultimate limit state condition (34). Capacity check is fulfilled if $\lambda_{b,j} \geq 1$.

As shown by [36], the supreme envelope amplified by $\lambda_{b,j}$ turns out to be internal and tangent to the bending capacity domain.

5.4. Comparison of the capacity check results

Capacity checks of Subsections 5.1, 5.2 and 5.3 have been carried out on the building models A–D represented in Figures 4 and 5; shear and bending checks have been performed on three cross section of each beam/column element, namely, at the two extremes and at the midspan section.

Contribution of the global torsion have been accounted for by means of the procedure summarized in Section 4 by assuming, as torsional spectrum, the DERS proposed in Section 3.1.

As basis of comparison, capacity checks have been carried out also by assuming no torsional spectrum and by shifting the structural masses, by the accidental eccentricity, at the locations represented in Figures 1(a) and 1(b). In such a case, since the mass locations are determined by the seismic input directions assumed to be oriented along global axes x and y, capacity checks are performed by adopting the elliptical envelope with $\theta = 0$.

Results of the capacity checks are compared by means of the logaritmic scatter plots represented in Figures 6 where the horizontal axis reports the critical multipliers $\lambda^e_{u,j}$, $\lambda^e_{s,j}$ and $\lambda^e_{b,j}$ computed by the mass shifting strategy for the interstorey drift, shear and bending capacity checks, respectively, while the vertical axis reports the values of the analogous critical multipliers $\lambda^d_{u,j}$, $\lambda^d_{s,j}$ and $\lambda^d_{b,j}$ computed by the application of the DERS.

The solid black line reported in the plots represents the equivalence condition between the mass shifting strategy and the application of the torsional response spectrum since its equation is $\lambda^d_{-} = \lambda^e_{-}$.

All points lying above the equivalence line represent the outcomes of those capacity checks for which the torsional spectrum procedure provides unconservative results with respect to the mass shifting strategy since the higher value of the critical multiplier means that the structural capacity is overestimated with respect to the standard code procedure. On the contrary, in the case of the points resulting below the equivalence line the torsional spectrum procedure turns out to be conservative with respect to the mass shifting strategy.

Capacity checks reported in Figures 6(a)–6(d) show that, adopting the DERS as torsional spectrum, the proposed procedure turns out to be, in general, more conservative than the mass shifting strategy since most of the points corresponding to the capacity checks lie below the equivalence line. In particular, all models show a fine equivalence concerning shear (red crosses) and bending (blue ribbons) capacity checks while for the case of the serviceability limit state (cyan diamonds) the torsional spectrum procedure provides more conservative results. Such a conservativeness increases as the structural model becomes more irregular.

To make a comparison with the responses of an alternative torsional spectrum, the proposed procedure has been performed by replacing the DERS with the SERS torsional spectrum presented in Section 3.2. The results of the relevant capacity checks are summarized in the scatter plots reported in Figures 7(a)–7(d) which are conceptually analogous to the previous plots in Figs. 6(a)–6(d). It is worth being noticed that, in this case, the capacity checks performed by the application of the SERS torsional spectrum turn out to be significantly unconservative with respect to the mass shifting strategy.

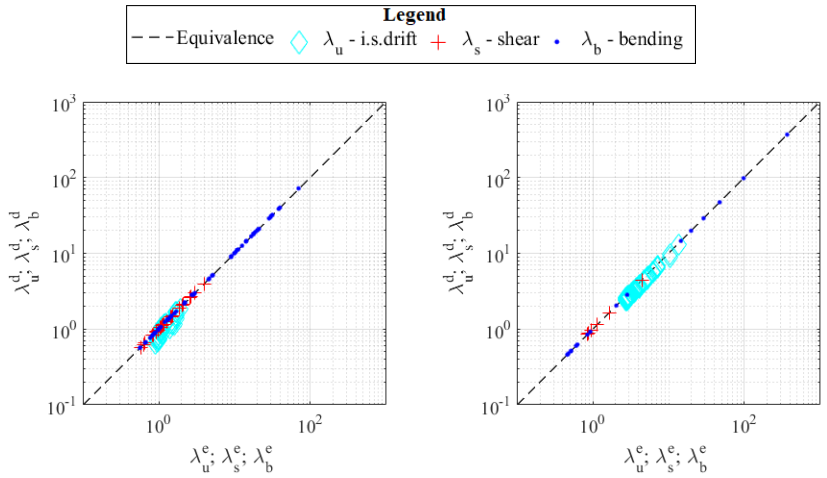

(a) Building A

(b) Building B

(c) Building C

(d) Building D

Figure 6: Scatter plot of the capacity check normalized multipliers computed by DERS

In particular, Figures 7(a)–7(d) show that there are cross sections for which the capacity check performed by the accidental eccentricity procedure is not fulfilled while the check performed by the application of SERS provides safe results.

To numerically investigate the performance of the proposed strategy, it is possible to define, for each capacity check, an error measurement as the percentage difference between the values of the critical multiplier computed by the proposed strategy and the mass shifting approach. Such a percentage error yields:

$$\mathcal{E}^{d}_{\cdot,j} = \frac{\lambda^{d}_{\cdot,j} - \lambda^{e}_{\cdot,j}}{\lambda^{e}_{\cdot,j}}; \quad \mathcal{E}^{s}_{\cdot,j} = \frac{\lambda^{s}_{\cdot,j} - \lambda^{e}_{\cdot,j}}{\lambda^{e}_{\cdot,j}} \tag{36}$$

where the dot $\cdot$ represents one of the considered limit state conditions u, s or b and j is the progressive index of the capacity check corresponding to a specific floor, for the case of serviceability limit state, or to a specific cross section, for the case of shear and bending checks.

Percentage error has been numerically evaluated for all the performed checks and Tables 3–5 report, for each building model, the average and the maximum value of $\mathcal{E}^{d}_{\cdot,j}$ and $\mathcal{E}^{s}_{\cdot,j}$.

Numerical estimates of the error relevant to the use of the proposed strategy in conjunction with DERS confirm that, for the case of serviceability capacity check (Table 3), the error average is negative while the error maximum value is not greater than 7% for all building models.

Error relevant to shear (Table 4) and to axial force - biaxial bending capacity checks (Table 5), performed by the proposed procedure in conjunction with DERS, presents very limited average and peak values, not exceeding 8%.

As a matter of fact, error estimates increase as the structural model becomes more irregular (buildings C and D). This aspect depends on the basic hypothesis characterizing the conventional single-storey oscillators used for computing the DERS. In fact, such oscillators approximate the structural behavior by means of two sole vibration modes related to horizontal translation global torsion, respectively. The significantly symmetric buildings A and B present a set of eigenvectors where vibration modes are clustered in triplets consisting of well-uncoupled modal shapes relevant either to one of the two horizontal translations or to the global torsion. For this reason, behavior of buildings A and B is particularly consistent with the features of the conventional oscillators.

On the contrary, modal shapes of the irregular buildings present a strong coupling between the two horizontal translations and the global torsion. For this reason, their behavior differs from the one assumed through the conventional oscillators what determines higher errors in absolute value.

For the reader's convenience, we recall that the strategy aims to define a conventional procedure to perform capacity check analyses using a single structural model and accounting for standard code provisions concerning accidental eccentricity. In this sense, its use can be accepted if the relevant results turn out to be conservative with respect to the mass shifting strategy or the error magnitude is limited so that it can be accepted as expected computational error.

A similar analysis of the numerical error has been performed by applying the proposed procedure in conjunction with the SERS torsional spectrum, whose outcomes are reported in Figure 7. The relevant error numerical estimates disclose an unconservative nature of SERS if used in conjunction with the proposed strategy. In particular, both average and peak values are significant for most of the building models and capacity check typologies.

Although SERS can be theoretically more significant than DERS, since it is consistent with a physical model of global torsion, as a matter of fact, overestimations greater than 50% of shear and bending capacity suggest that the spectrum fails in determining collapse multipliers consistently with the code requirements. Moreover, the SERS unconservative nature justifies the necessity of developing a specific rotational spectrum, the DERS, with the purpose of being used in conjunction with the proposed procedure in order to compute compliant seismic envelopes.

A final remark concerns capacity checks relevant to building B for which both the use of DERS and of SERS for the case of shear and bending capacity checks (Tabs. 4 and 5) present equal error values with magnitude $10^{-6}\%$. This issue is due to the fact that the structural model is particularly regular presenting, as main structural element, a squared-tube concrete kernel located in-plane at the geometrical center of the building. For this reason, global torsion does not influence the distribution of shear components and bending moments acting on the concrete kernel, where most of the capacity checks have been performed, since rotations about the vertical axis are balanced exclusively by the torque acting in the kernel. This is confirmed by the fact that serviceability capacity checks, reported in Table 3, present higher values of error averages and peaks since rotational displacements of the floors are determined by the torque stiffness of the kernel.

Capacity check of reinforced concrete with respect to torque actions has been not considered in this research because of the lack of reliable beam models accounting for the nonlinear behavior of concrete and the presence of steel reinforcing bars. Moreover, beam models approximate the kinematics of the kernel cross section which is assumed to remain plane. As shown by [40, 41] such a modeling custom, although capable of determining the global response of structural models

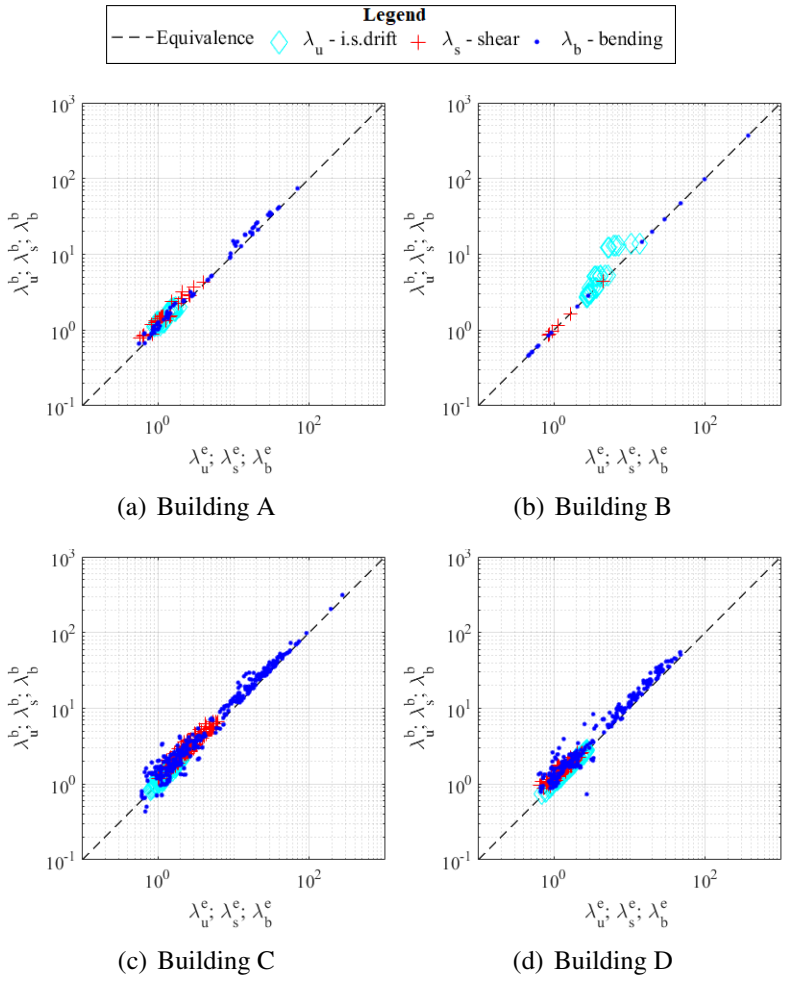

(a) Building A (b) Building B

(c) Building C (d) Building D

Figure 7: Scatter plot of the capacity check normalized multipliers computed by SERS

with sufficient accuracy, fails in accounting correctly for local phenomena and in accurately computing the stress distribution. The simplified beam-based model fulfills the aims of the present work since it permits to perform a consistent comparison between the outcomes of the proposed procedure and the mass shifting strategy.

A proper capacity check procedure accounting for the kernel torque should model kernels and shear walls by means of shell elements. As discussed in Section 6, the extension of the seismic envelopes to planar elements would be a significant

Table 3: Average and maximum values of the serviceability limit state capacity check percentage error

	$\mathcal{E}^d_{u,j}$ (DERS)		$\mathcal{E}^s_{u,j}$ (SERS)	
Building	average	maximum	average	maximum
A	-14.8%	-0.8%	17.6%	31.0%
B	-4.2%	-0.8%	21.0%	135.1%
C	-12.1%	6.3%	5.8%	25.2%
D	-15.0%	2.8%	3.5%	10.5%

Table 4: Average and maximum values of the shear ultimate limit state capacity check percentage error

	$\mathcal{E}^d_{s,j}$ (DERS)		$\mathcal{E}^s_{s,j}$ (SERS)	
Building	average	maximum	average	maximum
A	0.5%	1.2%	27.2%	58.2%
B	$6.5 \cdot 10^{-6}\%$	$8.5 \cdot 10^{-6}\%$	$9.6 \cdot 10^{-6}\%$	$9.7 \cdot 10^{-6}\%$
C	0.2%	0.7%	20.3%	60.2%
D	2.2%	5.5%	20.3%	58.8%

Table 5: Average and maximum values of the axial force - biaxial bending ultimate limit state capacity check percentage error

	$\mathcal{E}^d_{b,j}$ (DERS)		$\mathcal{E}^s_{b,j}$ (SERS)	
Building	average	maximum	average	maximum
A	0.9%	4.4%	14.8%	51.5%
B	$8.13 \cdot 10^{-6}\%$	$8.72 \cdot 10^{-6}\%$	$9.11 \cdot 10^{-6}\%$	$9.73 \cdot 10^{-6}\%$
C	0.6%	4.5%	22.5%	196.3%
D	2.3%	7.9%	25.7%	192.6%

enhancement for an exhaustive outset of the proposed procedure.

5.5. Comparison in terms of internal forces and node displacements

The conservative nature of the DERS is confirmed by the computation of the internal forces and displacement components involved in the capacity check procedure; conforming to the earthquake engineering practice, we present the results relevant to the bottom-left (SW) corner of the building plans. Figures 8 and 9 show the peak values of the u_x and u_y horizontal displacements due to the seismic excitation and computed by the mass shifting procedure (black lines), DERS (red

dash-dot line) and SERS (blue dashed line). In general, DERS provides greater horizontal displacements with respect to the mass shifting procedure for all the framed structural models while for building B it turns out to be slightly unconservative. Nevertheless, the magnitude of the error is very limited so that it can be accepted as modeling approximation.

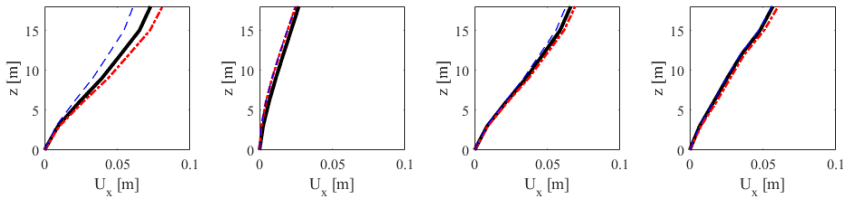

(a) Building A (b) Building B (c) Building C (d) Building D

Figure 8: Displacements u_x at the building SW corner computed by the mass shifting procedure (black line), the DERS (red dash-dot line) and the SERS (blue dashed line)

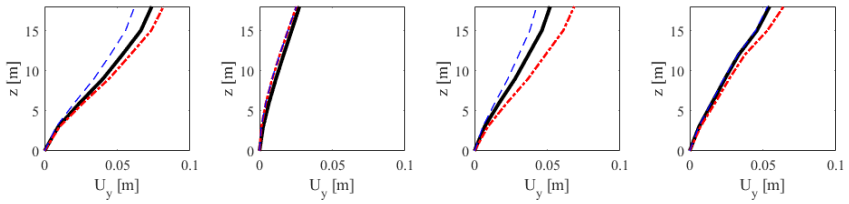

(a) Building A (b) Building B (c) Building C (d) Building D

Figure 9: Displacements u_y at the building SW corner computed by the mass shifting procedure (black line), the DERS (red dash-dot line) and the SERS (blue dashed line)

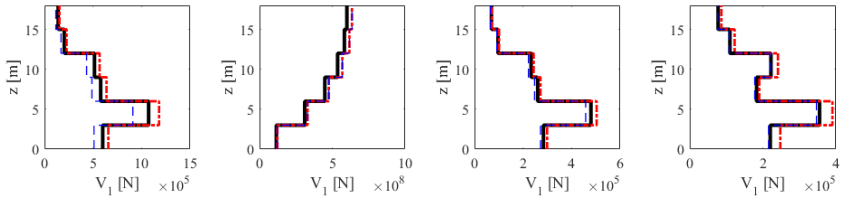

(a) Building A (b) Building B (c) Building C (d) Building D

Figure 10: Shear force T_1 of the Control Column computed by the mass shifting procedure (black line), the DERS (red dash-dot line) and the SERS (blue dashed line)

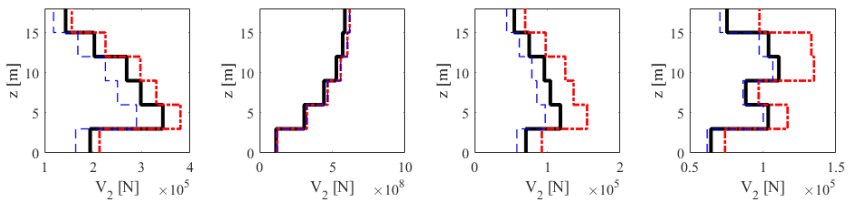

(a) Building A (b) Building B (c) Building C (d) Building D

Figure 11: Shear force T_2 of the Control Column computed by the mass shifting procedure (black line), the DERS (red dash-dot line) and the SERS (blue dashed line)

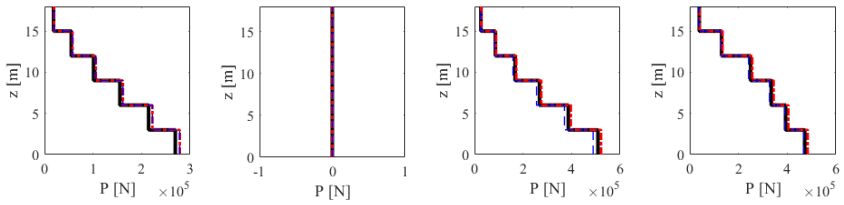

(a) Building A (b) Building B (c) Building C (d) Building D

Figure 12: Axial force P of the Control Column computed by the mass shifting procedure (black line), the DERS (red dash-dot line) and the SERS (blue dashed line)

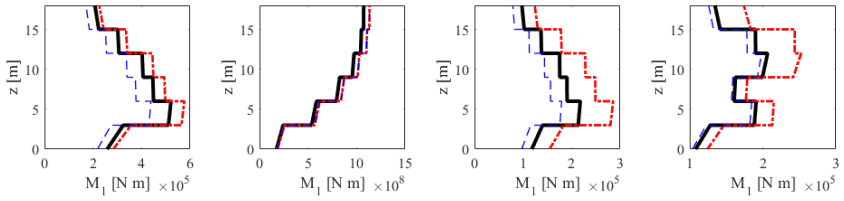

(a) Building A (b) Building B (c) Building C (d) Building D

Figure 13: Bending moment M_1 of the Control Column computed by the mass shifting procedure (black line), the DERS (red dash-dot line) and the SERS (blue dashed line)

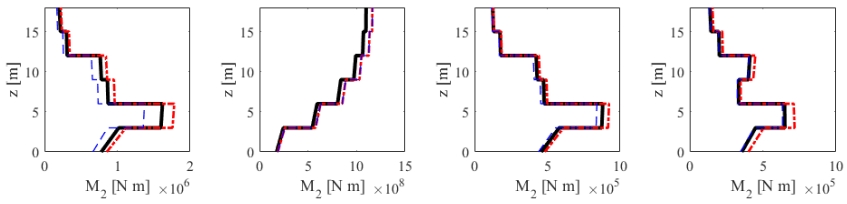

(a) Building A (b) Building B (c) Building C (d) Building D

Figure 14: Bending moment M_2 of the Control Column computed by the mass shifting procedure (black line), the DERS (red dash-dot line) and the SERS (blue dashed line)

On the contrary, SERS underestimates such responses for all the considered structural models and the magnitude of the error turns out to be significant for buildings A and C (see, e.g., Figures 9(a) and 9(c)).

A similar comparison has been performed in order to analyze the shear forces of the control columns reported in Figures 4(a), 4(b), 5(a) and 5(b). In particular, Figures 10 and 11 report the peak values due to the seismic excitations of the shear components V_1 and V_2, respectively, computed by the mass shifting procedure (black lines), DERS (red dash-dot line) and SERS (blue dashed line). Again, the DERS turns out to be conservative with respect to the mass shifting procedure for all the considered models while SERS provides unconservative results.

Analogous considerations can be made by comparing the seismic response in term of axial force and biaxial bending, reported in Figures 12, 13 and 14 respectively. Specifically, such figures report the peak values of the axial force P and of the bending moments M_1 and M_2 due to the seismic excitation and relevant to the control column computed by the mass shifting procedure (black lines), DERS (red dash-dot line) and SERS (blue dashed line). As for the case of shear, the DERS turns out to be conservative with respect to the mass shifting procedure while the SERS results unconservative especially for building A. In particular, the estimation of the axial force is not significantly sensitive to the accidental eccentricity; in fact, Figure 12 shows that the responses computed by DERS and SERS turn out to be almost identical to the ones evaluated by the mass shifting strategy. On the contrary, greater differences can be observed in the diagrams of the bending moments.

It is important to clarify that, although the trend hereby observed are qualitatively consistent with the outcomes of the capacity checks reported in Section 5.4, the magnitude of the errors with respect to the mass shifting procedure can be significantly different. In fact, the present comparisons present the peaks of each single seismic response without accounting for the vertical loads and, most important, for the correlation between different responses and for the variability of the seismic input angle. Conversely, the comparisons reported in Section 5.4, based upon the supreme envelope, do account for all these phenomena.

5.6. Qualitative comparison at a given cross section

In order to investigate the contribution of the rotational spectrum from a qualitative point of view, Figure 15 shows the seismic envelopes relevant to the axial force - biaxial bending response computed at the base cross section of the corner column of building A, which is highlighted in Fig. 4(a).

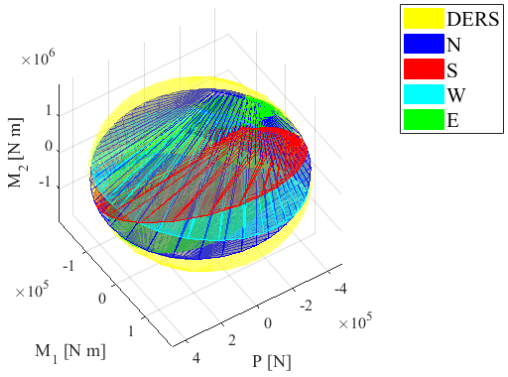

Figure 15: Axial force - biaxial bending seismic envelopes of the corner base section of building A computed by the DERS and by the mass–shifting procedure with floor masses assumed in locations N, S, W and E reported in Figures 1(a) and 1(b)

In particular, the yellow surface represents the supreme envelope computed by the application of the proposed procedure in conjunction with the DERS spectrum while the remaining surfaces represent the elliptical envelopes computed by the mass shifting strategy and relevant to the mass locations shown in Figures 1(a) and 1(b).

It is interesting to notice that the supreme envelope encompasses the elliptical envelopes obtained by the mass shifting. Therefore, points of the seismic response space which are contained within the supreme envelope but are external to the elliptical envelopes, correspond to capacity checks for which the proposed procedure turns out to be conservative with respect to the mass shifting strategy.

This phenomenon is even more evident for the case of the seismic envelopes represented in Figure 16(a) computed for the base section of the concrete kernel of building B. In such a case, the contribution of the axial force has been neglected since its component due to horizontal seismic loads turns out to be zero because of the structural symmetry.

In such a case, it is clear how the supreme envelope computed by the proposed procedure (yellow curve) encompasses the elliptical envelopes relevant to the mass shifting. Moreover, Figure 16(b) shows a similar comparison where masses have been shifted to the locations represented in Figure 1(c); in such a case, the elliptical envelopes turn out to be rotated of about $\pi/4$ with respect to the ones reported in Fig. 16(a) and are still contained within the supreme envelope. This suggests that the DERS procedure is capable of overcoming the needing of

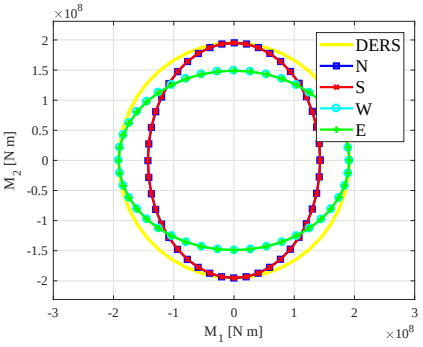

(a) Biaxial bending seismic envelopes of the kernel base section of building B computed by the DERS and the mass–shifting procedure with floor masses assumed in locations N, S, W and E reported in Figures 1(a) and 1(b)

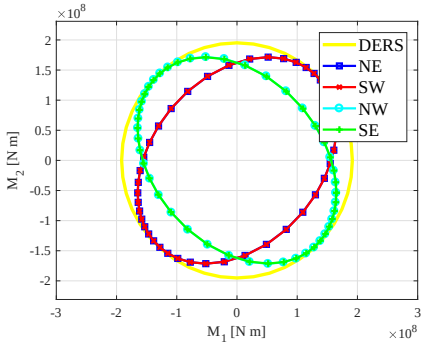

(b) Biaxial bending seismic envelopes of the kernel base section of building B computed by the DERS and the mass–shifting procedure with floor masses assumed in locations NE, SW, NW and SE reported in Figure 1(c)

Figure 16: Comparison of the biaxial bending seismic envelopes of the concrete kernel base section of building B computed by the DERS and the mass–shifting procedure with different mass locations

considering several mass locations depending on all the possible seismic input directions.

Clearly such a peculiar issue is due to the particular symmetry of building B and to the location of the considered cross section, which lies at the geometrical center of the structure. More generally, for some cross sections, it is possible that elliptical envelopes are not fully contained within the supreme envelope.

6. Conclusions

A computational procedure for performing response spectrum analysis of reinforced concrete structures by the use of seismic envelopes, defined by [28, 29], has been hereby presented. In particular, the strategy aims to fulfill the accidental eccentricity prescription of several structural codes, including Eurocode 8, by the use of a single structural model. In fact, the most widespread strategy for the application of the accidental eccentricity, consisting in shifting the structural masses along the axis orthogonal to the seismic input direction, results in at least four structural models if two ground motion components are adopted and compromises the chance of determining a unique seismic envelope of the structural

response.

The presented strategy has introduced an algorithmic response spectrum, the DERS, associated with a fictitious rotational ground motion about the vertical axis. It is determined by introducing two conventional single-storey oscillators whose parameters depend on some of the dynamic properties of the structure, such as the torsional frequency ratio, structural masses and the polar momentum of inertia. The first oscillator has mass shifted by the accidental eccentricity while the second one is subject to the DERS. An equivalence condition concerning the displacement responses of both oscillators, already exploited in the literature with the purpose of comparing recorded rotational spectra and accidental eccentricity prescriptions [10, 9], permits to compute the relevant values of the DERS in closed form.

Such an algorithmic spectrum is therefore introduced in the set of translational seismic excitations so that the traditional response spectrum analysis can be performed and the computation of the seismic envelopes of the structural response is straightforward.

The presented procedure has been numerically tested by analyzing four reinforced concrete structural models subject to the Eurocode 8 design spectrum and by comparing the relevant results with the outcomes of the traditional mass shifting procedure. In particular, each analysis consisted in performing capacity checks of the analyzed structures, by the procedure exploited by [36], with respect to three typologies of limit conditions: the serviceability limit state, defined by means of inter-story drift, the shear ultimate limit state and the axial force-biaxial bending ultimate limit state of the beam/column cross sections.

Moreover, in order to investigate the role played by the rotational spectrum in introducing global torsion effects, a further comparison has been performed by replacing the DERS with an alternative rotational spectrum, denoted as SERS, derived by the investigation presented by [3] which is one of the few contributions which permits to define a direct relationship between accidental eccentricity and a rotational ground motion.

The numerical results of the performed capacity checks show that the proposed strategy used in conjunction with DERS turns out to be either equivalent or conservative with respect to the mass shifting procedure for all the analyzed structures. In fact, values of the critical multiplier relevant to the capacity check, computed by the proposed strategy, turn out to be, in general, smaller than the corresponding critical multipliers computed by the mass shifting procedure. Unconservative outcomes of the proposed strategy, although noticed in the numerical results, are relevant to a limited set of capacity checks and their relative error is

not greater than 10%. The highest absolute-values of the error relevant to DERS are attained for the two irregular buildings. This is due to the significantly different behavior of the irregular structures with respect to the one of the conventional oscillators.

Critical multipliers obtained by replacing DERS by the SERS spectrum show that capacity checks result unconservative with respect to the mass shifting procedure with non-negligible values of the error, especially for the case of the regular models, and peaks up to 196%.

The fact that capacity checks performed by SERS provide significantly unconservative results justified the necessity of developing a specific torsional spectrum, the DERS, suitable for the proposed procedure of structural analysis.

The conservative nature of the proposed procedure with respect to the mass shifting strategy does not compromise its use in structural design because it fulfills the standard code prescriptions. This last aspect is of outmost importance: procedures alternative to the mass shifting, although more significant from a physical and theoretical point of view as well as computationally efficient, cannot be used in those countries, such as Italy, in which structural codes assume mandatory nature. This is the case of the results relevant to the use of the SERS rotational spectrum which, yet based on a significant theoretical basis, would not provide a structural capacity adequate to the code requirements.

Despite of the fact that the proposed computational strategy permits the use of the seismic envelopes for structural design in common practice, further developments are currently under investigation. In particular, future research will focus on the enhancement of the axial force - biaxial bending capacity check algorithm, still requiring a high computational effort, by introducing a characterization of the capacity domain by means of Minkowski sum of ellipsoids. Such a numerical tool proved to be significantly efficient from a computational point of view as well as particularly feasible for representing capacity domains of reinforced concrete cross sections [37].

Moreover, further investigations will concern the modeling of the torsionally flexible building presenting a concrete kernel located at the center of its plan which has been modeled by beam elements. As discussed in Section 5.6, the use of shell elements is preferable in order to compute more accurate results. Current research is focused on the implementation in the presented procedure of the seismic envelope formulation for plane elements, presented by [25, 26], and already used for similar purposed by [18].

Funding

The present research was supported by the Italian Government – PRIN 2015 grants [2015JW9NJT-PE8, WP2 Task 2.1] – which is gratefully acknowledged by the authors.

AppendixA. Response spectrum analysis of the coupled oscillator

The response spectrum analysis of the coupled oscillator presented in Section 3.1 consists in the computation of the eigenvectors and eigenvalues of the matrix:

$$\mathbf{A} = \mathbf{M}^{-1}\mathbf{K} = \begin{bmatrix} \omega^2 & \dfrac{\omega^2\varepsilon}{r} \\ \dfrac{\omega^2\varepsilon}{r} & \omega^2\Omega^2 + \dfrac{\varepsilon^2}{r^2} \end{bmatrix} \tag{A.1}$$

Since the 2-DOFs oscillator is very simple, spectral analysis can be performed in closed form. Specifically, the eigenvalues λ_j^2 and eigenvectors $\mathbf{\Lambda}_j$ of $\mathbf{A}$ are:

$$\lambda_1^2 = c - R; \quad \lambda_2^2 = c + R \tag{A.2}$$

$$\mathbf{\Lambda}_1 = \begin{bmatrix} \omega^2\varepsilon/r \\ -\left(\omega^2 + R - c\right) \end{bmatrix}; \quad \mathbf{\Lambda}_2 = \begin{bmatrix} -\left(\omega^2 + R - c\right) \\ -\omega^2\varepsilon/r \end{bmatrix} \tag{A.3}$$

where two auxiliary variables have been introduced for convenience:

$$c = \omega^2\frac{1 + \Omega^2 + \varepsilon^2/r^2}{2}; \quad R = \frac{\omega^2}{2}\sqrt{\left(\Omega^2 + \varepsilon^2/r^2 - 1\right)^2 + 4\varepsilon^2/r^2} \tag{A.4}$$

Recalling that eigenvalues λ_1 and λ_1 are modal pulsations, the corresponding modal periods are:

$$T_1 = \frac{2\pi}{\lambda_1} = \frac{2\pi}{\sqrt{c - R}}; \quad T_2 = \frac{2\pi}{\lambda_2} = \frac{2\pi}{\sqrt{c + R}} \tag{A.5}$$

moreover, given the pseudo–acceleration response spectrum $S_\chi(T)$, the corresponding displacement spectrum $D_\chi(T)$ is:

$$D_\chi(T) = \frac{S_\chi(T)}{\left(2\pi/T\right)^2} \tag{A.6}$$

so that the displacement translational response spectrum values $D_{\chi,1}$ and $D_{\chi,2}$ corresponding to the two eigenvalues λ_1 and λ_1 are:

$$D_{\chi,1} = \frac{S_\chi\left(2\pi/\sqrt{c-R}\right)}{c-R}; \quad D_{\chi,2} = \frac{S_\chi\left(2\pi/\sqrt{c+R}\right)}{c+R} \tag{A.7}$$

where $S_\chi(T)$ represents the pseudo–acceleration response spectrum.

Furthermore, recalling that the mass matrix in the equation of motion (13) has unit entries, the modal participation factors are:

$$\gamma_{\chi\,1} = \frac{\mathbf{\Lambda}_1^T \begin{bmatrix} 1 \\ 0 \end{bmatrix}}{\mathbf{\Lambda}_1^T \mathbf{\Lambda}_1} = \frac{\omega^2 \varepsilon / r}{\omega^4 \varepsilon^2 / r^2 + \left(-\omega^2 + c - R\right)^2}; \quad \gamma_{\chi\,2} = \frac{\mathbf{\Lambda}_2^T \begin{bmatrix} 1 \\ 0 \end{bmatrix}}{\mathbf{\Lambda}_2^T \mathbf{\Lambda}_2} = \frac{-\omega^2 + c - R}{\omega^4 \varepsilon^2 / r^2 + \left(-\omega^2 + c - R\right)^2} \tag{A.8}$$

Therefore, the peak value of the response ru_θ due to the rotation only is:

$$\max\left(ru_\theta\right) = \left[D_{\chi,1}^2 \gamma_{\chi\,1}^2 \Lambda_{1,2}^2 + D_{\chi,2}^2 \gamma_{\chi\,2}^2 \Lambda_{2,2}^2 + D_{\chi,1} D_{\chi,2} \gamma_{\chi\,1} \gamma_{\chi\,2} \Lambda_{1,2} \Lambda_{2,2} \rho_{1,2}\right]^{0.5} \tag{A.9}$$

where $\Lambda_{i,j}$ denotes the j–th component of vector $\mathbf{\Lambda}_i$ and $\rho_{1,2}$ is the modal correlation coefficient of the CQC superposition rule reported in Equation (17).

On account of Equations (A.3)–(A.8) and recalling coefficients c_1 and c_2 in Equation (19), Equation (A.9) becomes:

$$\max\left(ru_\theta\right) = \frac{c_1 c_2}{c_1 + c_2} \sqrt{D_{\chi,1}^2 - D_{\chi,2}^2 - D_{\chi,1} D_{\chi,2} \rho_{1,2}} \tag{A.10}$$

It is worth being emphasized that such a procedure can be performed as long as the eigenvalues (A.2) are both positive. Such a condition is always fulfilled because matrix $\mathbf{A}$ in Eq. (A.1) is positive-definite.

References

[1] Alfano, G., Marmo, F., Rosati, L., 2007. An unconditionally convergent algorithm for the evaluation of the ultimate limit state of RC sections subject to axial force and biaxial bending. International Journal for Numerical Methods in Engineering 72, 924–963.

[2] Annigeri, S., Mittal, A. K., Jain, A. K., 1996. Uncoupled frequency ratio in asymmetric buildings. Earthquake Engineering & Structural Dynamics 25 (8), 871–881.

[3] Basu, D., Constantinou, M. C., Whittaker, A. S., 2014. An equivalent accidental eccentricity to account for the effects of torsional ground motion on structures. Engineering Structures 69 (0), 1 – 11.

[4] Basu, D., Jain, S., 2004. Seismic analysis of asymmetric buildings with flexible floor diaphragms. Journal of Structural Engineering 130 (8), 1169–1176.

[5] Chen, S. F., Teng, J. G., Chan, S. L., 2001. Design of biaxially loaded short composite columns of arbitrary section. Journal of Structural Engineering 127 (6), 678–685.

[6] Chopra, A., 2007. Dynamics of Structures: Theory and Applications to Earthquake Engineering. Pearson/Prentice Hall.

[7] Chopra, A., 2007. Elastic response spectrum: A historical note. Earthquake engineering & structural Dynamics 36 (1), 3–12.

[8] De La Llera, J., Chopra, A., 1995. Estimation of accidental torsion effects for seismic design of buildings. Journal of Structural Engineering 121 (1), 102–114.

[9] De La Llera, J. C., Chopra, A. K., 1994. Accidental torsion in buildings due to base rotational excitation. Earthquake Engineering & Structural Dynamics 23 (9), 1003–1021.

[10] De La Llera, J. C., Chopra, A. K., 1994. Evaluation of code accidental–torsion provisions from building records. Journal of Structural Engineering 120 (2), 597–616.

[11] De La Llera, J. C., Chopra, A. K., 1994. Using accidental eccentricity in code-specified static and dynamic analyses of buildings. Earthquake engineering & structural Dynamics 23 (9), 947–967.

[12] Der Kiureghian, A., 1981. A response spectrum method for random vibration analysis of mdf systems. Earthquake Engineering & Structural Dynamics 9 (5), 419–435.

[13] Eurocode 2, 1992. CEN EN 1992–1–1 Design of concrete structures – Part 1-1: General rules and rules for buildings.

[14] Eurocode 8, 1998. CEN EN 1998–1 Design of structures for earthquake resistance. Part I: General rules, seismic actions and rules for buildings.

[15] Goel, R., Chopra, A., 1993. Seismic code analysis of buildings without locating centers of rigidity. Journal of Structural Engineering - ASCE 119 (10), 3039–3055.

[16] Hernández, J. J., López, O. A., 2002. Response to three-component seismic motion of arbitrary direction. Earthquake Engineering & Structural Dynamics 31 (1), 55–77.

[17] ICBO, 1991. Uniform building code. In: International Conference of Building Officials, Pasadena (CA).

[18] Ile, N., Frau, A., 2017. Use of response envelopes for seismic margin assessment of reinforced concrete walls and slabs. Nuclear Engineering and Design 314, 238–250.

[19] Karimiyan, S., Kashan, A., Karimiyan, M., 2014. Progressive collapse vulnerability in 6-Story RC symmetric and asymmetric buildings under earthquake loads. Earthquake and Structures 6 (5), 473–494.

[20] Lin, W. H., Chopra, A. K., De La Llera, J. C., 2001. Accidental torsion in buildings: Analysis versus earthquake motions. Journal of Structural Engineering 127 (5), 475–481.

[21] López, O., Hernández, J., Bonilla, R., Fernández, A., 2006. Response spectra for multicomponent structural analysis. Earthquake Spectra 22 (1), 85–113.

[22] Marmo, F., Rosati, L., 2012. Analytical integration of elasto-plastic uniaxial constitutive laws over arbitrary sections. International Journal for Numerical Methods in Engineering 91, 990–1022.

[23] Marmo, F., Rosati, L., 2013. The fiber-free approach in the evaluation of the tangent stiffness matrix for elastoplastic uniaxial constitutive laws. International Journal for Numerical Methods in Engineering 94, 868–894.

[24] Marmo, F., Serpieri, R., Rosati, L., 2011. Ultimate strength analysis of prestressed reinforced concrete sections under axial force and biaxial bending. Computers & Structures 89, 91–108.

[25] Menun, C., 2003. A response–spectrum–based envelope for Mohr's circle. Earthquake Engineering & Structural Dynamics 32 (12), 1917–1935.

[26] Menun, C., 2004. An envelope for Mohr's circle in seismically excited three-dimensional structures. Earthquake Engineering & Structural Dynamics 33 (9), 981–998.

[27] Menun, C., Der Kiureghian, A., 1998. A Replacement for the 30%, 40%, and SRSS Rules for Multicomponent Seismic Analysis. Earthquake Spectra 14 (1), 153–163.

[28] Menun, C., Der Kiureghian, A., 2000. Envelopes for Seismic Response Vectors. – I: Theory. Journal of Structural Engineering 126 (4), 467–473.

[29] Menun, C., Der Kiureghian, A., 2000. Envelopes for Seismic Response Vectors. – II: Application. Journal of Structural Engineering 126 (4), 474–481.

[30] NBCC, 2005. National Research Council of Canada – National Building Code of Canada (NBCC). Ottawa (ON), Canada.

[31] Newmark, N. M., 1969. Torsion in symmetrical buildings. In: Proceedings of the Fourth World Conference on Earthquake Engineering, Santiago, Chile, 1969. pp. (3) 19–32.

[32] NTC, 2008. CSLLPP – DMLLPP 14/01/2008 Norme Tecniche per le Costruzioni – Standard building rules. Roma, Italy.

[33] NTC, 2018. CSLLPP – DMLLPP 17/01/2018 Norme Tecniche per le Costruzioni – Standard building rules. Roma, Italy.

[34] NZS 1170.5, 2004. Standards New Zealand NZS 1170.5 – Structural design actions, Part 5: Earthquake actions. New Zealand.

[35] Selna, L. G., Lawder, J. H., 1977. Biaxial inelastic frame seismic behavior. In: Publ SP Am Concr Inst SP-53, Symp on Reinf Concr Struct in Seism Zones; Am Concr Inst Annu Conv, San Francisco, Calif;. pp. 439–461.

[36] Sessa, S., Marmo, F., Rosati, L., 2015. Effective use of seismic response envelopes for reinforced concrete structures. Earthquake Engineering & Structural Dynamics 44 (14), 2401–2423.

[37] Sessa, S., Marmo, F., Rosati, L., Leonetti, L., Garcea, G., Casciaro, R., 2018. Evaluation of the capacity surfaces of reinforced concrete sections: Eurocode versus a plasticity-based approach. Meccanica 53 (6), 1493–1512.

[38] Smeby, W., Der Kiureghian, A., 1985. Modal combination rules for multi-component earthquake excitation. Earthquake Engineering & Structural Dynamics 13 (1), 1–12.

[39] Tso, W. K., Dempsey, K. M., 1980. Seismic torsional provisions for dynamic eccentricity. Earthquake Engineering & Structural Dynamics 8, 275–289.

[40] Valoroso, N., Marmo, F., Sessa, S., 2014. Limit state analysis of reinforced shear walls. Engineering Structures 61, 127–139.

[41] Valoroso, N., Marmo, F., Sessa, S., 2015. A novel shell element for nonlinear pushover analysis of reinforced concrete shear walls. Bulletin of Earthquake Engineering 13 (8), 2367–2388.

[42] Wilson, E. L., Der Kiureghian, A., Bayo, E. P., 1981. A replacement for the srss method in seismic analysis. Earthquake Engineering & Structural Dynamics 9 (2), 187–192.